Journal of Materials Chemistry A

Accepted Manuscript

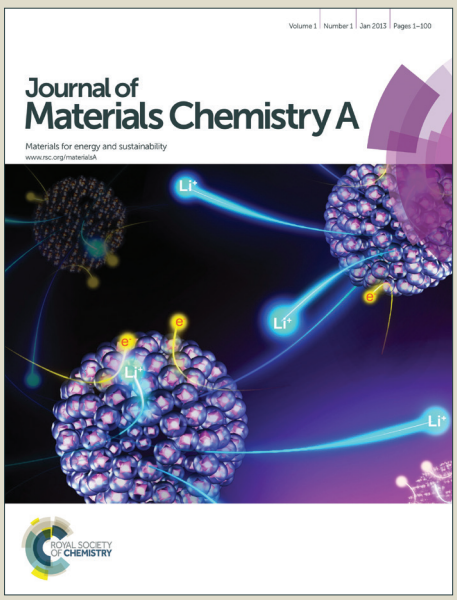

ROYAL SOCIETY OF CHEMISTRY

www.rsc.org/materialsA

Cite this: DOI: 10.1039/c0xx00000x

www.rsc.org/xxxxxx

ARTICLE TYPE

Dynamics of semiconducting nanocrystals uptake into mesoporous TiO_2 thick films by electrophoretic deposition

Lei Jin,[a] Haiguang Zhao,[a,b] Dongling Ma,[a] Alberto Vomiero,*[a,b,c] Federico Rosei*[a,d]

Received (in XXX, XXX) Xth XXXXXXXXX 20XX, Accepted Xth XXXXXXXXX 20XX

DOI: 10.1039/b000000x

Electrophoretic deposition (EPD) is a simple technique for the uptake of nanoparticles into mesoporous films, for example to graft semiconducting nanocrystals (quantum dots, QDs) on mesoporous oxide thick films acting as photoanodes in third generation solar cells. Here we study the uptake of colloidal QDs into mesoporous TiO_2 films using EPD. We examined PbS@CdS core@shell QDs, which are optically active in the near infrared (NIR) region of the solar spectrum and exhibit improved long-term stability toward oxidation compared to their pure PbS counterpart, as demonstrated by X-ray photoelectron spectroscopy (XPS) and photoluminescence (PL) spectroscopy. We applied Rutherford backscattering spectrometry (RBS) to obtain Pb depth profile into the TiO_2 matrix. EPD duration in the range from 5 to 120 min and applied voltages from 50 to 200 V were considered. The applied electric field induces the fast anchoring of QDs to the oxide surface. Consequently, QD concentration in the solution contained in the mesoporous film drastically decreases, inducing a Fick-like diffusion of QDs. We modelled the entire process as a QD diffusion related to the formation of QD concentration gradient, and a depth-independent QD anchoring, and were able to determine the electric field-induced diffusion coefficient *D* for QDs and the characteristic time for QD grafting, in very good agreement with experiment. *D* increases from $(1.5\pm0.4)\times10^{-5}$ μm^2 s^{-1} at 50 V to $(1.1\pm0.3)\times10^{-3}$ μm^2 s^{-1} at 200 V. The dynamics of EPD may also be applied to other different colloidal QD and quantum rod materials for sensitization of mesoporous films. These results quantitatively describe the process of QD uptake during EPD, and can be used to tune the optical and optoelectronic properties of composite systems, which determine, for instance, the photoconversion efficiency in QD solar cells (QDSCs).

INTRODUCTION

An intense worldwide effort is geared towards developing third generation photovoltaic (PV) cells, to obtain low cost, high efficiency and environmentally friendly devices by using wet chemistry synthetic routes for the preparation of suitably tailored nanomaterials. [1 - 10] One of the most promising solar cell architectures is based on quantum dots (QDs).[1-5,11] QD solar cells (QDSCs) benefit from the ability to tune the optical properties of QDs by manipulating their size and composition. [12 , 13] In particular, QDs that are optically active in the near infrared (NIR) spectral region, such as PbS [14] and PbSe [15] have attracted enormous interest as light absorbers, because they can allow to extend the absorption band toward the NIR part of the solar spectrum. This interest was recently renewed after achieving a photoconversion efficiency (PCE) above 7%, by using NIR PbS QDs.[16] In a particular configuration of QDSCs,[17] the QDs are grafted to the surface of a wide band gap semiconductor.[18,19] The QDs absorb light and an exciton is created. Then exciton dissociation occurs at the QD/oxide interface, and the resulting electron is injected into the oxide that acts as electron transporter.[20] A liquid electrolyte completes the electrochemical system and allows QD neutralization after electron injection. For this reason, a major challenge is to apply a low-cost process to incorporate QDs onto the oxide and to achieve effective QD-electrode junctions that promote charge separation, while minimizing surface charge trapping and losses.

In situ growth methods have been widely used to obtain QD-decorated TiO_2 photoanodes, including chemical bath deposition (CBD),[21,22] and successive ionic layer adsorption and reaction (SILAR).[23,24,25] Although a direct contact between the oxide and the QDs is achieved in this way, there is no independent control of QD coverage and size.[4] These drawbacks can be avoided if QDs are synthesized before sensitization in the form of colloids, and then grafted onto oxide surface. Typically, three main different techniques are used to couple pre-synthesized QDs with oxide thick films: linker-assisted adsorption,[22,26] direct adsorption (DA),[27] and electrophoretic deposition (EPD).[28] In most cases, the attachments of the QDs to the mesoporous electrode is achieved by using a molecular linker between QD and the oxide particle, and up to several days are needed to achieve the desired coverage and photoanode optical density for QDs with hydrophobic ligand.[12] In the case of hydrophilic ligands, QD uptake is typically much faster (several hours),[29] but the linker

molecule may act as an additional barrier for electron injection, affecting the photovoltaic properties.[30] Even though the ligands on colloidal QDs surfaces may act as charge transfer barriers, efficient charge transfer can still take place based on our previous studies.[31,32] The DA method is based on solvent/non-solvent precipitation of QDs from the solution into the mesoporous film: the tendency of the QDs to agglomerate in solution may lead to uneven and polydisperse surface coverage.[33] EPD, a widely used technique, is based on the motion and grafting of charged particles under an applied electric field, and presents several advantages over other methodologies, such as low cost, short fabrication time, simple equipment and formation of a uniform QD layer of controlled thickness[34,35] even on flexible plastic substrates.[36-39]

EPD was previously employed to deposit semiconducting,[40,41] metallic,[42,43] and insulating[44,45] nanoparticles on conductive substrates or polymer films.[43,46] The first application of EPD for solar cells was reported for the deposition of TiO_2 nanoparticles.[44] Colloidal CdSe QDs were deposited via EPD on a flat thin film as a proof of concept for PV applications, yielding low PCEs (~10^{-6} %) due to the very low absorbance (i.e. optical density) of the solar cell.[47] To increase the active area, CdSe QDs were incorporated into porous TiO_2 layers several microns thick,[28] reaching efficiencies as high as 1.7%, under 1 sun illumination. Mora-Seró and co-workers[48] prepared QDSCs by depositing colloidal PbS and PbSeS QDs on TiO_2 mesoporous films via EPD. A strong relationship between QD size, EPD time and device performance was observed, clearly identifying the factors in EPD that are essential for the optimization of QDSCs. In addition, the decrease of recombination resistance with EPD time unambiguously demonstrated that conformal coverage of TiO_2 with QDs would reduce charge recombination from TiO_2 to the electrolyte.[49] For these reasons, suitable control of the parameters determining QD uptake and oxide coverage is mandatory. However, so far, only generic demonstrations of almost constant QD depth profiling into films is claimed, based on low-resolution EDX analysis,[47] and no systematic investigation of QD uptake is found in the literature.

On the other hand, another challenge in this kind of PV devices is the development of long-term stable QDSCs. QDs, due to their large surface-to-volume ratio, are very sensitive to surface defects and oxidation, which cause charge trapping,[50] leading to a decrease in PCE.[51] For this reason, QDs were typically capped by organic surface ligands,[52,53] while the dangling bonds remaining on the QD surface can act as carrier trapping sites if partial ligand un-passivation occurs.[54,55] Recent studies[56,57,58] revealed that a robust, larger band gap inorganic shell can provide more complete passivation for the QD surface, contributing to largely improved chemical, thermal, photochemical stability, and an acceptable charge injection rate in QDs with suitable core size and shell thickness.[7,31]

Here, we report a systematic investigation of the dynamics of NIR QDs inserted into TiO_2 mesoporous film via EPD. We used PbS@CdS core@shell QDs as highly stable light harvesters and investigated the influence of EPD time (5 to 120 min) and voltage (50 to 200 V) on the QD uptake process. The optical density of the obtained film is strongly dependent on the applied voltage, the deposition time and the concentration of solution containing the QDs (Figure S1). We modelled the deposition process using Fick's diffusion law and explained the observed trends as a fast (and depth-independent) QD uptake induced by the presence of the electric field, followed by a diffusion-induced QD migration from outside the film, due to the fast creation of a QD concentration gradient. In addition, we demonstrated the increased stability of the core@shell structure compared to PbS QDs in terms of structure and optical properties, based on X-ray photoelectron spectroscopy (XPS) and PL measurements. Thanks to the much higher stability of the core@shell QDs as compared to standard pure PbS QDs, our findings suggest that the PbS@CdS QDs loaded with EPD can be exploited for the development of highly efficient and stable light absorbers in PV devices.

EXPERIMENTAL SECTION

Materials.

Lead chloride (98%), sulfur (100%), oleylamine (OLA) lead acetate trihydrate, trioctylphosphine (TOP 90%), bis (trimethylsilyl) sulfide $(TMS)_2S$, (technical grade, 70%), cadmium oxide (99%), oleic acid (OA), mercaptoacetic acid (MAA), 1-octadecene (ODE), acetonitrile, and hydrochloric acid were obtained from Sigma-Aldrich Inc. Hexane, toluene, and ethanol were purchased from Fisher Scientific Company. Titania paste consisting of ~20 nm nanoparticles in diameter was supplied by Dyesol (18 NR-T, Queanbeyan, Australia). All chemicals were used as purchased.

QDs and TiO_2 film preparation.

Synthesis of PbS QDs. PbS QDs were synthesized using OLA as ligand.[58] Typically, in a three-neck reaction flask, $PbCl_2$ (36 mmol) in OLA (24 mL) and sulphur (3.6 mmol) in OLA (5 mL) were purged by N_2 at room temperature for 30 min. Then, the $PbCl_2$-OLA suspension was heated up to 160 °C and kept at this temperature for 1 hour. The $PbCl_2$-OLA suspension was then cooled down to 120 °C under vacuum for 15 min. The flask was then reopened and the N_2 flux was restored. Sulphur in OLA at room temperature was quickly injected into the $PbCl_2$-OLA suspension under vigorous stirring. The growth reaction was conducted at 100 °C for 1–5 min followed by removal of the heating mantle and quenching to room temperature using a cold water bath. The purification procedure was carried out in air. Hexane (20 mL) and ethanol (40 mL) were added to the crude solution followed by centrifugation to separate the QDs. The pure PbS QDs capped with OLA were then re-dispersed in OA/toluene (1/20 V/V). After precipitation with ethanol and centrifugation, the QDs were re-dispersed in toluene and the exchange was repeated twice. Finally, the QDs were dispersed in toluene. The size of synthesized PbS QDs can be tunable from 3.4 nm to 6 nm by adjusting the molar ratio of Pb/S, injection temperature and growth time.[58]

PbS QDs with diameter 3.0 nm were synthesized with hot injection method by using OA as ligands.[59] Typically, a mixture of lead acetate trihydrate (1 mmol), OA (1.2 mL), TOP (1 mL), and ODE (15 mL) were heated to 150 °C for 1 h. Then, the system was cooled down to ~100 °C under vacuum for 15 min. Subsequently, a sulphur precursor solution was prepared by mixing $(TMS)_2S$ (0.5 mmol) with 0.2 mL of TOP and 4.8 mL of

the mixture was quickly injected into the reaction flask at 130 °C; subsequently the reaction was quenched by cold water. PbS QDs were precipitated with ethanol, centrifuged to remove unreacted lead oleate and free OA molecules and then re-dispersed in toluene.

Synthesis of PbS@CdS QDs. PbS@CdS QDs were synthesized via a cation exchange method.[58] Typically, CdO (2.3 mmol), OA (2 mL) and ODE (10 mL) were heated to 255 °C under N_2 for 20 min. The clear solution was cooled down to 155 °C under vacuum for 15 min. The flask was then reopened and the N_2 flux was restored. PbS QDs suspension in toluene (1 mL, Absorbance = 3 at the first exciton peak) was diluted in 10 mL toluene, bubbled with N_2 for 30 min and then immediately heated to 100 °C. The Cd/OA mixture was added via a syringe. The solution was maintained at 100 °C for 1-30 minutes and then cooled down to room temperature with cold water. PbS@CdS QDs with tunable core sizes and shell thickness in the range 0.2–0.5 nm were synthesized by choosing different starting PbS sizes together with different reaction parameters (Pb-to-Cd ratio and reaction time).

For both PbS and PbS@CdS systems we introduce the labels "S", "M" and "L" indicating the small, medium and large size, according to QD dimensions reported in Table 1.

TiO_2 film preparation. Fluorine doped tin oxide (FTO) coated glass substrates (Pilkington, bought from Hartford Glass Co. Inc., USA) with sheet resistance 15 Ω/square were cleaned with ethanol, thoroughly rinsed with deionized water and dried in a filtered air stream. Subsequently the titania paste (composed of 20 nm diameter anatase nanoparticles, Dyesol 18NR-T) was deposited on the top of FTO by tape casting and dried in air for 10 min. The photoanodes were then fired on a hot plate at 80 ℃ for 60 min, followed by sintering at 450 ℃ for 30 min, forming a transparent film. Film thickness was measured using a stylus profilometer.

EPD of the QDs on the TiO_2 film. QDs were dispersed in toluene, with a pair of TiO_2 FTO slides vertically immersed in the QDs solution and facing each other. The distance between them was adjusted at 1 cm and the deposition area of the electrodes was about 0.72 cm^2. A voltage of 50-200 V was applied for 5-120 min. To wash off unbound QDs after the EPD process, the samples were rinsed several times with toluene and dried with N_2 at room temperature. We focused on the analysis of QDs uptaken on the positive electrode of the EPD system.

Characterization

QDs were dispersed in toluene to acquire absorption spectra using a Cary 5000 UV-visible-NIR spectrophotometer (Varian) with a scan speed of 600 nm/minute. The composition of the films was measured on a freshly cleaved cross-section of the TiO_2 layers after EPD, using an Atmospheric Thin Window (ATW) energy dispersive X-ray spectroscopy (EDX) detector in FEI Sirion high resolution scanning electron microscope (HRSEM) system operated at 10-15 kV accelerating voltage, whose resolution is 133 eV at 5.9 keV. The morphology of QDs was analyzed with a JEOL 2100F transmission electron microscope (TEM) before and after grafting to TiO_2. For observation of TiO_2 after QDs grafting, the QD/TiO_2 system was transferred onto TEM grids by simple mechanical scratching of the thick film. Fluorescence spectra (PL) were taken with a Fluorolog®-3 system (Horiba Jobin Yvon) using an excitation wavelength of 670 nm. The concentration of samples was adjusted so as to their optical densities were below 0.2 at the chosen excitation wavelength. QDs were also drop casted on silicon substrate to form thin films for comparison with QDs loaded on TiO_2 film by EPD. XPS was performed in a VG Escalab 220i-XL equipped with hemispherical analyzer recorded for a Twin Anode X-Ray Source. The spectra acquisition parameters (channel exposition, number of scans, analyzer parameters, etc.) were selected so as to provide the best energy resolution and signal/noise ratio. Pb 4f and C 1s photoelectron lines were acquired during the experiment. The C 1s peak (BE = 284.6 eV) was used as an internal reference line to accurately determine the positions of other spectral lines. The fine structure of the photoelectron lines was treated using Casa XPS software (2.3.15 Version). Rutherford backscattering (RBS) was carried out using a $^4He^+$ beam under the following experimental conditions: E_0=5.1 MeV; beam geometry: IBM; normal incidence of the beam on sample surface; scattering angle $\theta = 140^o$. The RUMP Code was used to simulate the RBS spectra. The density of the TiO_2 mesoporous films was calculated by dividing their areal density (obtained from RBS) by their thickness, measured through a stylus profilometer.

RESULTS AND DISCUSSION

Synthesis and characterization of QDs in solution and in TiO_2 films

Colloidal PbS QDs and PbS@CdS QDs of diameters ranging between 2.9-4.1 nm were synthesized and then dispersed in toluene, with typical QY of 40~80%. We selected three different sizes of QDs: 3.0±0.3 nm, 3.6±0.3 nm, 4.0±0.3 nm and compared pure PbS and core@shell PbS@CdS with similar diameters (the representative size distribution for sample of PbS_M and PbS@CdS_M are shown in Figure S5). The size of the QDs was chosen to be smaller than the mesopores of the TiO_2 film, to allow QD penetration into the film during EPD, which would be otherwise inhibited.

The absorption spectra of differently sized PbS and PbS@CdS QDs dispersed in toluene are shown in Figure 1 (a). The average PbS diameters for PbS QDs and the average PbS core size for the core@shell QDs are determined from the position of the first excitonic absorption peak.[60] CdS shell thickness in PbS@CdS QDs can be obtained by simply subtracting the PbS core size from the overall size of PbS@CdS QDs based on TEM observations. In our previous work,[60] we demonstrated that the shell of PbS@CdS QDs is mainly composed of CdS. The overall QD diameter (d_{total}), core diameter (d_{core}), CdS shell thickness (d_{shell}), the position of the first excitonic absorption peak and PL peak are listed in Table 1.

As-synthesized QDs were then loaded on mesoporous TiO_2 layers by EPD. TiO_2 film thickness was around ~6 μm, estimated using a stylus profilometer. SEM was also carried out on the cross section of selected samples (see Figure 1 (c)) to compare the thickness values obtained respectively by profilometry and SEM, which agreed within the experimental errors. After EPD of QDs, both the positive and negative TiO_2 electrodes were colored, consistently with previous studies,[28,48] indicating the deposition of negatively and positively charged QDs. According

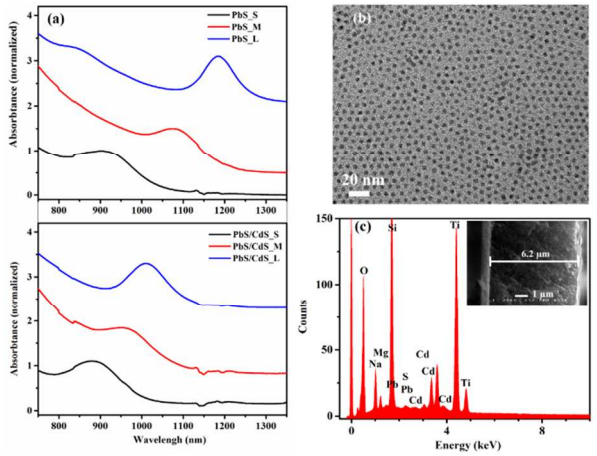

Figure 1. Absorption spectra of (a) PbS (top) and PbS@CdS QDs (bottom) in solution before EPD. (b) Representative TEM image of PbS@CdS QDs. (c) EDX analysis of PbS@CdS QDs with ~3.0 nm core diameter and shell thickness of ~0.2 nm after anchoring to TiO_2 nanoparticles by using EPD at 200 V for 30 min. Inset: SEM cross-section of a TiO_2 film.

Table 1. Dimensions and optical properties of pure and core@shell QDs investigated in this study. The overall size of PbS@CdS QDs is determined based on TEM observation, the core size is estimated from the position of the first excitonic peak and the shell thickness is estimated by simple subtraction. To identify the different samples, S M L labels are used according to their small, medium and large size, respectively.

Sample	Diameter (nm)	Core Diameter (nm)	Shell thickness (nm)	Abs max (nm)	PL max (nm)
PbS_S	3.09±0.3	3.09	0	912	
PbS_M	3.69±0.3	3.69	0	1079	
PbS_L	4.11±0.3	4.07	0	1184	
PbS@CdS_S	3.12±0.3	2.98	0.10±0.03	879	920
PbS@CdS_M	3.68±0.3	3.26	0.20±0.05	961	1075
PbS@CdS_L	4.10±0.3	3.44	0.30±0.05	1012	1180

to previous work,[61] the initial positive charge in nanocrystals can be understood in terms of the preferential removal of ligand, which exposes Pb (or Cd for core@shell) sites at the surface. It may also make QDs more "sticky" by reducing the solubilization energy in the solvent, and may facilitate charge transfer at the electrode surfaces. The origin of the negatively charged nanocrystals can be explained with S-rich surfaces or surface reconstruction upon the loss of the passivating ligand molecules, which exposes S atoms.[62, 63] The effective deposition of QDs into the TiO_2 is confirmed by EDX, Figure 1 (c)) in SEM (inset of Figure 1 (c)), in which the signal from Cd, Pb and S are clearly visible.

Figure 2 displays TEM images of a TiO_2 electrode sensitized with core@shell PbS@CdS at different EPD times. The EPD process produces a well-separated dispersion of core@shell QDs on TiO_2 and the QD coverage becomes denser at increasing EPD time (Figure 2 (d)). No obvious QD aggregation occurs, which could be detrimental for electron transfer from QDs to TiO_2 in the operating device.

QD Stability after EPD

To estimate the effect of EPD on the stability of the structure and optical properties of QDs, we performed XPS and PL analyses of selected QDs deposited on a silicon substrate or after

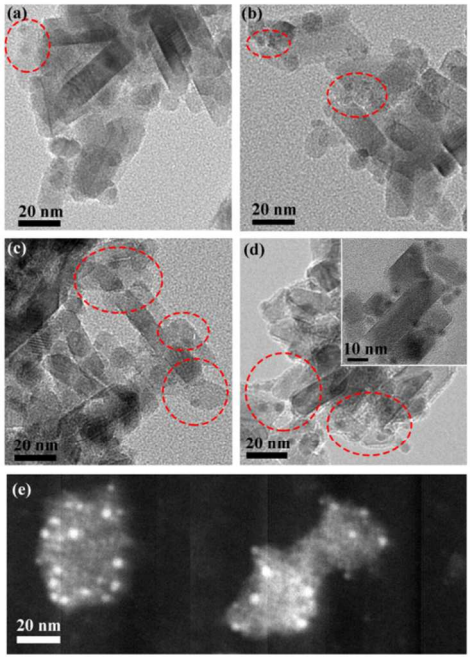

Figure 2. Representative TEM images of PbS@CdS QDs loaded into TiO_2 at four different EPD durations: (a) 10 min (b) 30 min (c) 60 min (d) 120 min. Inset of (d): enlarged TEM image. The red circles highlight the presence of the QDs. (e) Dark field Scanning TEM image of TiO_2 nanoparticles covered by QDs. The high contrast between the TiO_2 and QDs allow precise identification of the position of the QDs on the surface of TiO_2 nanoparticles.

EPD on TiO_2 mesoporous films. We compared QDs with and without CdS shell to test the ability of the shell to prevent QD degradation.

XPS was used to characterize the effect of EPD on the chemical bonds in QDs. The results are reported in Figure 3. The high resolution spectrum of Pb 4f in PbS QDs on silicon reveals the presence of Pb 4f 7/2 (137.9 eV) and Pb 4f 5/2 (142.7 eV), respectively, from Pb-S bonds, and also two higher energy components (138.5 eV for Pb 4f 7/2 and 143.3 eV for Pb 4f 5/2), which can be originated from the interaction between Pb and OA ligands.[60] After EPD, the high energy peaks of Pb 4f totally disappear, and two additional lower energy components appear at 136.6 eV for Pb 4f 7/2 and 141.4 eV for Pb 4f 5/2 of PbS (Figure 3 (a)), which might be attributed to the presence of Pb dangling bonds due to the unpassivated Pb atoms on the QD surface, as a result of EPD.[60] The interaction between the QDs and TiO_2 NPs is the likely reason for the shift of Pb-S bond to higher energies, from 137.9 eV to 138.1 eV for Pb 4f 7/2 and from 142.7 eV to 142.9 eV for Pb 4f 5/2. The high resolution spectrum of Pb 4f in PbS@CdS QDs on silicon (Figure 3 (b)) presents two additional higher binding energy peaks, similar to PbS QDs on silicon, slightly less intense than in PbS QDs. This feature very likely implies the presence of an interaction between a small amount of unpassivated Pb atoms on the QD surface and ligands, as well as oxygen in aerobic environments. Some PbS@CdS QDs might have an incomplete CdS shell, leaving some portion of Pb atoms at the surface. After EPD, in contrast to pure PbS, the two additional higher binding energy peaks almost maintained the same position as those of QDs on silicon, indicating that for the core@shell structure, there is no detectable formation of dangling

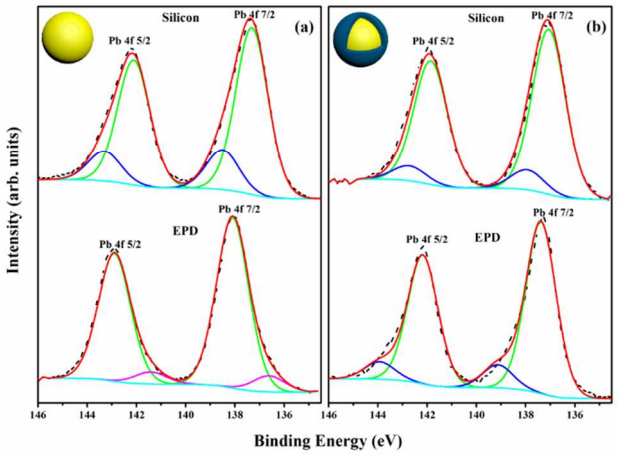

Figure 3. High resolution Pb 4f core level spectra after correction of electrostatic charging obtained from (a) PbS_M quantum dot (b) PbS@CdS_M core@shell QDs on silicon (up) and upload into TiO_2 with EPD (down). (d) 120 min.

bonds, contrary to what happened in pure PbS QDs. These results clearly suggest an increased stability of the existing chemical bonds and surface structures of core@shell QDs with respect to pure PbS QDs.

PL spectra of TiO_2 samples after EPD of PbS and PbS@CdS QDs, 3.6 nm in size, are reported in Figure 4 (a) and (b), respectively. Quantum confinement in QDs results in size-dependent band gap, inducing size dependent PL. The PL peak position of pure PbS QDs after EPD (1175 nm) has a blue shift (32 nm) compared to pure PbS in solution (1207 nm), indicating the shrinking of the PbS core during uptake, due to surface oxidation, as explained below. After 24 hours exposure to air, the PL peak position further blue shifts (~138 nm) compared to pure PbS QDs in solution, probably due to PbS oxidation. In fact, oxidation reduces the size of un-oxidized PbS, which is the source of PL, thus causing a blue shift of the PL signal due to the shrink of the emitting PbS volume. In addition, the peak width is quite broad (~212 nm) with respect to that in solution (~141 nm), indicating the presence of trap-related emission, consistently with the presence of un-passivated dangling bonds confirmed by XPS (Figure 3 (a)) or with trap states in formed oxides. In PbS@CdS core@shell QDs, almost no shift of the PL peak was recorded, even after exposing the sample to air for 24 h (Figure 4 (b)), clearly demonstrating the increased optical stability thanks to the presence of the passivating shell.

Dynamics of EPD

The increased stability of core@shell QDs motivated us to select this structure to investigate the dynamics of QDs uptaken during EPD. We selected the PbS@CdS_L QDs for the purpose. We applied RBS to reconstruct the depth profile of QDs inside the TiO_2 matrix. The RBS spectrum of a typical sample after EPD is reported in Figure 5. The signals from Ti and Pb are clearly visible, allowing quantitative analysis of in-depth distribution of Pb into the TiO_2 layer. The red curve is the RUMP code simulation, including also the contribution from FTO substrate (broad peak from the Sn signal in the region between channel 350 and 450), demonstrating that very accurate depth profiling of Pb is possible in this kind of samples. The signal from Cd is masked

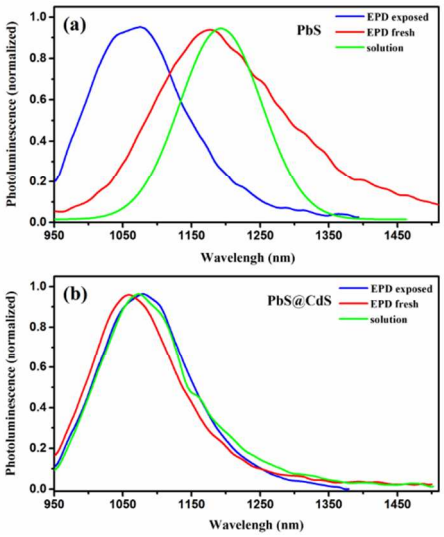

Figure 4. PL of (a) PbS_M QDs and (b) PbS@CdS_M QDs just after EPD and after 24 hours exposure to air. Benchmarking PL spectra of QDs in solution is also reported.

by Pb. For this reason, we focused on the depth profiling of Pb, under the hypothesis that the core-shell structure and Pb:Cd atomic ratio is preserved after EPD and so, in principle, Cd depth profile is the same as Pb.

Figure 5 (b) focuses on the RBS spectral range related to Pb. Two different regions can be clearly identified: region A, representing the inner part of the film at the TiO_2/FTO interface, and region B, which represents the exterior part of the film, close to the surface. In region A, the concentration of Pb is almost constant and depth-independent, and increases exponentially with EPD time (see Figure S2). Pb is present even at very short EPD times, indicating that the solution containing QDs penetrates the entire film depth from the beginning of the process and that QDs start attaching to TiO_2 over the entire depth of the film. In region B, a surface Pb peak is present after 5 min EPD deposition. Subsequently Pb enters the film during EPD. Pb surface concentration increases with the time up to a saturation concentration (see Figure S3).

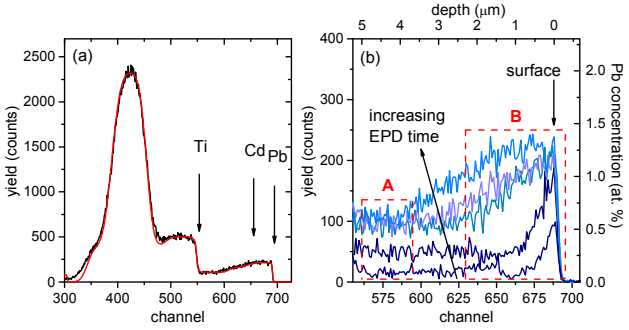

Figure 5. (a) RBS spectrum of TiO_2 mesoporous film sensitized with QDs for 120 minutes at 200 V EPD bias. The red curve is the RUMP code simulation. The surface edges for Ti, Cd and Pb are indicated by arrows. (b) RBS signal of the spectral region pertaining Pb signal for samples sensitized at different durations (5, 10, 30, 60, 120 minutes, from dark blue to light azure) under 200 V bias. A and B rectangles highlight the two different regions in which QD diffusion cannot be detected (A) or is clearly visible (B).

We estimated the main Pb parameters as a function of EPD

time from the RBS spectra: (i) Pb atomic concentration at the surface (surface peak in region B); (ii) Pb atomic concentration at the interface with FTO (from region A); (iii) penetration depth of Pb (x_0, presented in Figure 6 (a) and in Figure S4). $C(x,t)$ is the atomic concentration of Pb as a function of the position inside the film and the EPD time t, and $C_s(t)$ and $C_i(t)$ Pb are the atomic concentration at the surface of the film and at the FTO/TiO_2 interface, respectively. x_0 is defined as:

$$C(x_0,t)-C_i(t)=\frac{C_s(t)-C_i(t)}{2} \qquad (Equation\ 1)$$

Figure 6 (a) and (b) report x_0 as a function of the EPD time and square root of EPD time, respectively. The parameter x_0 exhibits linear dependence on the square root of the EPD time. Such dependence is typical of diffusion processes driven by Fick's diffusion, [64] in which the penetration depth presents a square root dependence on diffusion time and is regulated by a diffusion coefficient D, according to the following equation:

$$\frac{C(x_0,t)-C_i}{C_s-C_i}=1-erf\left(\frac{x}{2\sqrt{Dt}}\right) \qquad (Equation\ 2)$$

In a typical Fick's diffusion phenomenon (see $\frac{C(x_0,t)-C_i}{C_s-C_i}=1-erf\left(\frac{x}{2\sqrt{Dt}}\right)$ (*Equation* 2), the parameters C_i and C_s are time-independent, since the concentration of the diffusing element is constant at the surface source and in the bulk at infinite distance from the surface. [64]

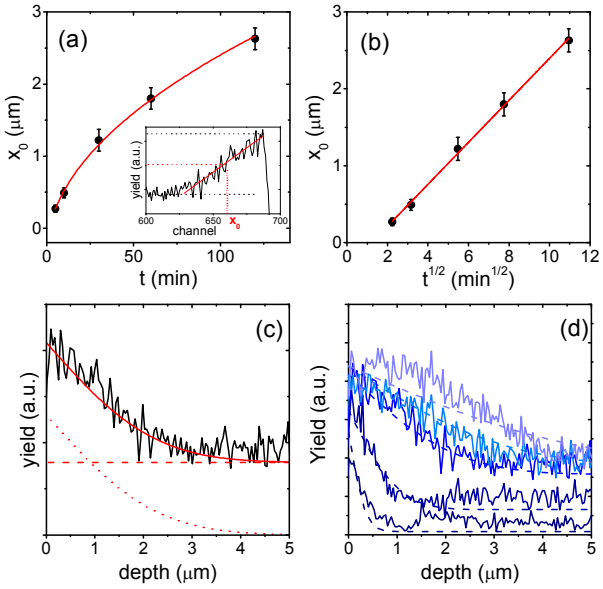

Figure 6. (a) Position of the parameter x_0 as a function of EPD time. Inset: illustration of the procedure to determine x_0 from a standard RBS spectrum. (b) Parameter x_0 versus square root of EPD time. (c) Experimental Pb yield (black line) versus film depth and simulated yield (red solid line) obtained from the diffusion coefficient D and the characteristic decay time τ obtained from RBS data. The two different components contributing to the curve are reported: diffusion process of Pb from solution (red dotted line) and position-independent QD uptake (red dashed line). (d) Experimental (solid lines) and simulated (dashed lines) Pb yields for the complete series of EPD samples under 200 V bias.

However, in the present case, both C_i and C_s are dependent on EPD time, as clearly visible from the experiment, not allowing a straightforward application of Fick's second law to EPD. In addition, the process under investigation is not a simple diffusion process, since our system is composed of various mutually interacting elements: the solution, in which QDs are dispersed; the TiO_2 host, in which QDs can attach; the external electric field, which provides attachment of QDs. In addition, we are not able to detect the QDs diffusing in the solution, but the QDs attached to the oxide. For all these reasons, an adequate description of the experimental results requires a few assumptions on the physical and chemical processes that occur during EPD.

At the beginning of the EPD, QD concentration is constant inside the solution which permeates the mesoporous film. The application of the external electric field induces the attachment of QDs to TiO_2. This process causes the decrease of QD concentration in the solution inside the TiO_2 mesoporous layer, while QD concentration outside TiO_2 film remains constant. We quantitatively estimated the decrease of QD concentration in the solution permeating the film from the amount of Pb in region A of the RBS spectrum: as already mentioned, Pb concentration in region A exhibits an exponential growth up to an asymptotic limit (Figure S2). The characteristic time of the process is $\tau=(11.5\pm0.5)$ min. We correlate the asymptotic Pb concentration to the total amount of charged QDs in solution (which are supposed to be the QDs available for grafting during EPD): once all the charged QDs present in solution are attached to the oxide, no more QDs are available, the solution inside TiO_2 is almost empty and the concentration of PbS attached to TiO_2 reaches its (maximum) asymptotic limit. TEM results (Figure 2) clearly show that TiO_2 coverage is not complete and Pb concentration in region B (higher than in region A) demonstrates that further QD uptake is possible, if enough QDs are present in solution. In addition, EPD tests at different voltages indicate that the asymptotic Pb concentration is almost independent on the applied electric field, within the experimental error (see Table 2), supporting again the hypothesis of complete QD depletion of the solution inside the film within the first minutes of EPD.

Table 2. PbS concentration and diffusion coefficient D as a function of the applied voltage in EPD.

Applied voltage (V)	Pb at.% (surface)	Pb at.% (interface)	D (10^{-3} μm^2 s^{-1})
50	1.20±0.1	0.55±0.05	(1.1±0.3)
100	0.95±0.05	0.50±0.05	(0.12±0.03)
200	0.60±0.05	0.40±0.05	(0.015±0.004)

The decrease of QD concentration inside the solution contained in the TiO_2 film creates a concentration gradient that induces QD diffusion from the solution outside the film, into the solution inside the film. Once the QDs enter the film, they can attach to the TiO_2 surface due to the action of the electric field.

An empirical description of Pb concentration as a function of EPD time and of the position inside the film assumes that the process of QD uptake at the beginning of EPD, and the process of QD diffusion due to the rise of QD concentration gradient are mutually independent.

Under this hypothesis, the concentration C(x,t) can be written as follows:

$$C(x,t)=C_0\left[1-\exp\left(-\frac{t}{\tau}\right)\right]+C_1\left[1-erf\left(\frac{x}{2\sqrt{Dt}}\right)\right] \qquad (Equation\ 3)$$

The first part accounts for position-independent QD uptake from original solution and the second part takes into account QD diffusion from the surface and successive QD uptake. This assumption oversimplifies the problem, since the two processes are correlated. However, the agreement between the proposed solution and the experimental findings is excellent, as visible in Figure 6 (d), in which the experimental data (solid lines) are interpolated using $C(x,t) = C_0\left[1-\exp\left(-\frac{t}{\tau}\right)\right] + C_1\left[1-erf\left(\frac{x}{2\sqrt{Dt}}\right)\right]$ (*Equation 3* (dashed lines).

In the interpolation, C_0, τ, C_1, and D are experimentally determined. C_0 is the asymptotic Pb concentration in region A after 120 minutes EPD, τ is calculated from the Pb atomic concentration in region A as a function of time (Figure S2), C_1 is the asymptotic Pb concentration at the surface of the TiO_2 film, and D is the diffusion coefficient estimated from the linear fit of Figure 6 (b).

A reconstruction of Pb depth profiling versus EPD time is reported in Figure 7, based on *Equation 3*. The concentration gradient created at the surface, due to the depletion of solution inside TiO_2 is well visible, as well as the evolution of PbS depth profile leading to the final concentration after long (in the range of hours) EPD.

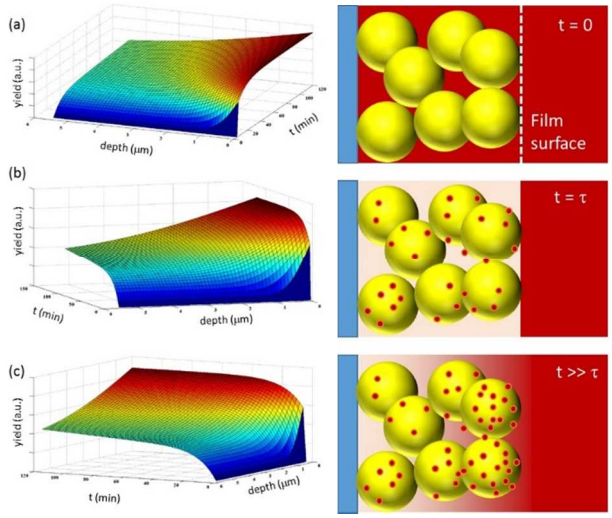

Figure 7 Pb distribution versus time and depth in TiO_2 film under three different perspectives, based on the experimental parameters calculated for 200 V applied bias.

We extended the investigation of EPD to different applied voltages from 50 V to 200 V. Figure 8 shows the parameter x_0 versus the square root of EPD time (Figure 8 (a)), the diffusion coefficient versus EPD bias (Figure 8 (b)), and the fitting of three Pb profiles after 60 min EPD at three different voltages (Figure 8(c)). For all the applied biases, x_0 exhibits a linear dependence on the square root of the EPD time, with the slope increasing at increasing bias. Accordingly, D is dependent on the applied voltage and, in particular, it increases from $(1.5\pm0.4)\times10^{-5}$ μm^2 s^{-1} at 50 V to $(1.1\pm0.3)\times10^{-3}$ μm^2 s^{-1} at 200 V. The increase in D reflects in Pb depth profiling, as is visible in Figure 8 (c), in which the Pb profile is reported for three different voltages after 60 min EPD. The interpolating curves after 60 min EPD were based on the experimental results on C_i, C_s and τ as reported in Table 2.

During EPD, the motion of QDs inside the mesoporous film and QD attachment are two different processes. RBS only provides information about the QD present on the oxide surface after grafting, yet we are unable to study the motion of QDs before they are grafted to the oxide, because there is no experimental technique to obtain an on-line monitoring of QD depth profile during EPD. This means that the information about QD motion inside the film is mediated by the process of QD attachment, under the hypothesis that the characteristic time for grafting does not depend on QD concentration. There may be a dependence of the characteristic grafting time with the applied voltage, but we are not able to discriminate this dependence and the dependence of QD motion.

In addition, the previous achievements allow us, by simple integration, to determine the quantity of Pb entering TiO_2 at the beginning of the process through the pristine solution, and the quantity of Pb diffusing from the external solution inside the film. The fraction of Pb entering the film due to diffusion is reported in Figure 8 (d) for three different applied voltages as a function of EPD time. The application of 50 V induces negligible diffusion, and the amount of QD is almost due to QD uptake directly from the pristine solution. As soon as the applied voltage increases, the fraction of Pb coming from diffusion increases. At 200 V, after 120 min, more than 40% of the Pb decorating the TiO_2 comes from diffusion from the external solution, indicating that this process cannot be neglected during the preparation of this kind of composite systems.

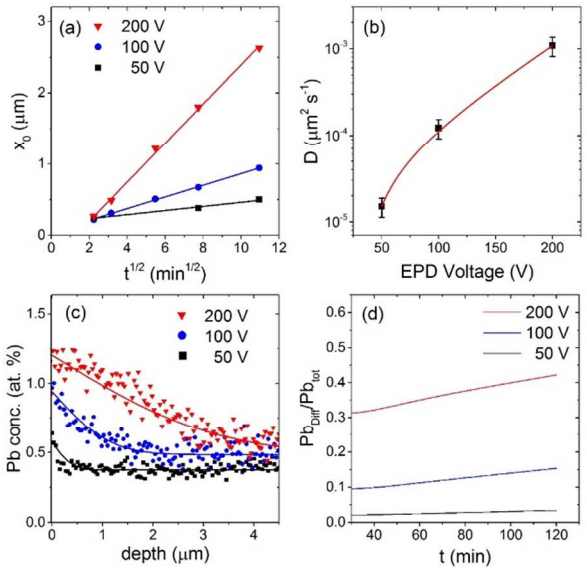

Figure 8 (a) x_0 versus square root of EPD time. (b) Diffusion coefficient D versus EPD voltage, and (c) Pb concentration versus depth at three different EPD voltages after 60 min EPD. Symbols: experiment; solid lines: simulations according to the values of D reported in Table 2. (d) Fraction of Pb introduced in the film by diffusion (Pb_{Diff},) at different voltages. Pb_{Diff} and the total Pb amount are calculated as the integral of Pb concentrations along film depth based on the two components illustrated in Figure 6 (c).

CONCLUSIONS AND PERSPECTIVES

In summary, we investigated the upload of *ex situ* core@shell NIR colloidal QDs into mesoporous TiO_2 films by EPD. We demonstrated good electrode coverage without QD aggregation and improved stability of core@shell QDs towards oxidation and

defect formation after EPD, compared to pure PbS QDs. We studied the dynamics of EPD uptake by RBS. The entire process can be rationalized as follows: First, QD concentration is constant inside the solution inserted into the mesoporous film, and the applied electric field induces attachment of QDs to TiO_2. Then, depletion of QD in solution induces the formation of a QD concentration gradient inducing a Fick's-like diffusion. The diffusion coefficient *D* exhibits an electric field enhancement, which is still not completely clear and needs to be further investigated. These results clearly demonstrate that QD uptake can be fine-tuned by controlling the main EPD parameters, and give rational and quantitative description of preparation of QD sensitized photoanodes for QDSCs. These results can be applied for the optimization of QD sensitization of mesoporous films for QDSCs and can be used, in principle, for other kinds of semiconducting nanocrystals commonly employed to sensitize mesoporous electrodes.

Acknowledgements

The authors are grateful to R. Milan and I Concina for their support in the set-up of the EPD system, and to M. Chicoine and S. Roorda for their support on ion beam analysis. We acknowledge funding from NSERC in the form of Discovery Grants (D.M. and F.R.) and a Strategic Project Grant. F.R. is grateful to the Canada Research Chairs program for partial salary support. This work was partially funded by MDEIE through the international project WIROX. H.Z. is grateful to NSERC for a personal post-doctoral fellowship. A.V. thanks the European Commission for an individual Marie Curie Fellowship under contract n° 299490 and partial support under EC contract WIROX n° 295216. F.R. acknowledges NSERC for an E.W.R. Steacie Memorial Fellowship.

Notes and references

a Institut National de la Recherche Scientifique, 1650 Boulevard Lionel-Boulet, Varennes, J3X 1S2, Québec, Canada. Prof. Federico Rosei E-mail: rosei@emt.inrs.ca
b CNR-INO SENSOR Lab, Via Branze 45, 25123 Brescia, Italy.
c Luleå University of Technology, 971 98 Luleå, Sweden. Prof. Alberto Vomiero E-mail: alberto.vomiero@ltu.se
d Center for Self-Assembled Chemical Structures, McGill University, H3A 2K6 Montreal, Quebec, Canada

1 A. Zaban, O. I. Mićić, B. A. Gregg and A. J. Nozik, *Langmuir,* 1998, **14**, 3153–3156.
2 A. J. Nozik, *Phys. E,* 2002, **14**, 115–120.
3 P. V. Kamat, *J. Phys. Chem. C,* 2008, **112**, 18737–18753.
4 H. Lee, H. C. Leventis, S. J. Moon, P. Chen, S. Ito, S. A. Haque, T. Torres, F. Nüesch, T. Geiger, S. M. Zakeeruddin, M. Grätzel, and M. K. Nazeeruddin, *Adv. Funct. Mater.,* 2009, **19**, 2735–2742.
5 I. J. Kramer, E. H. Sargent, *ACS Nano,* 2011, **5**, 8506–8514.
6 L. Yi, Y. Liu, N. Yang, Z. Tang, H. Zhao, G. Ma, Z. Sua and D. Wang, *Energy Environ. Sci.*, 2013,**6**, 835−840.
7 H. Sun, J. He, J. Wang, S. Y. Zhang, C. Liu, T. Sritharan, S. Mhaisalkar, M. Y. Han, D. Wang and H. Chen, *J. Am. Chem. Soc.* 2013, **135**, 9099−9110,
8 N. Yang, Y. Liu, H. Wen, Z. Tang, H. Zhao, Y. Li and D. Wang, *ACS Nano*, 2013, **7**(2), 1504–1512.
9 L. Yi, D. Wang and M. Gao, *Cryst. Eng. Comm.*, 2012, **14**, 401–404.
10 Y. Cui, X. Lai, L. Li, Z. Hu, S. Wang, J. E. Halpert, R. Yu, D. Wang, *ChemPhysChem* , 2012, **13**, 2610.
11 I. Concina, M. M. Natile, M. Ferroni, A. Migliori, V. Morandi, L. Ortolani, A. Vomiero and G. Sberveglieri, *ChemPhysChem*, 2011, **12**, 863-870.
12 I. Robel, V. Subramanian, M. Kuno and P. V. Kamat, *J. Am. Chem. Soc.,* 2006, **128**, 2385–2393.
13 A. Kongkanand, K. Tvrdy, K. Takechi, M. Kuno and P.V. Kamat, *J. Am. Chem. Soc.,* 2008, **130**, 4007–4015.
14 M. C. Beard, A. G. Midgett, M. Law, O. E. Semonin, R. J. Ellingson, A. J. Nozik, *Nano Lett.,* 2008, **8**, 3488–3492.
15 R. Debnath, J. Tang, D. A. Barkhouse, X. Wang, A. G. Pattantyus-Abraham, L. Brzozowski, L. Levina and E. H. Sargent, *J. Am. Chem. Soc.,* 2010, **132**, 5952–5953.
16 G. I. Koleilat, I. J. Kramer, C. T. O. Wong, S. M. Thon, A. J. Labelle, S. Hoogland and E. H. Sargent, *Sci. Rep.,* 2013, **3**, 2166.
17 A. Braga, S. Giménez, I. Concina, A. Vomiero, and I. Mora-Seró, *J. Phys. Chem. Lett.,* 2011, **2** (5), 454–460.
18 Y. L. Lee, B. M. Huang and H. T. Chien, *Chem. Mater.,* 2008, **20**, 6903–6905.
19 O. Niitsoo, S. K. Sarkar, C. Pejoux, S. Ruhle, D. Cahen and G. Hodes, *J. Photochem. Photobiol. A,* 2006, **181**, 306–313.
20 A. G. Pattantyus-Abraham, I. J. Kramer, A. R. Barkhouse, X. Wang, G. Konstantatos, R. Debnath, L. Levina, I. Raabe, M. K. Nazeeruddin, M. Grätzel, E. H. Sargent, *ACS Nano,* 2010, **4**, 3374–3380.
21 L. J. Diguna, Q. Shen, J. Kobayashi and T. Toyoda, *Appl. Phys. Lett.,* 2007, **91**, 023116.
22 I. Mora- Seró, S. Giménez, F. Fabregat-Santiago, R. Gomez, Q. Shen, T. Toyoda and J. Bisquert, *Acc. Chem. Res.,* 2009, **42**, 1848–1857.
23 S. Hachiya, Q. Shen and T. Toyoda, *J. Appl. Phys.,* 2012, **111**, 104315.
24 S. S. Mali, S. K. Desai, S. S. Kalagi, C. A. Betty, P. N. Bhosale, R. S. Devan, Y. R. Ma and P. S. Patil, *Dalton Trans.,* 2012, **41**, 6130–6136.
25 I. Concina, N. Memarian, G. S. Selopal, M. M. Natile, G. Sberveglieri, A. Vomiero, *J. Power Sources*, 2013, **240**, 736–744.
26 D. R. Baker and P. V. Kamat. *Adv. Funct. Mater.,* 2009, **19**, 805–811.
27 S. Giménez, I. Mora-Seró, L. Macor, N. Guijarro, T. Lana-Villarreal, R. Gómez, L. J. Diguna, Q. Shen, T. Toyoda and J. Bisquert, *Nanotechnology,* 2009, **20**, 295204.
28 A. Salant, M. Shalom, I. Hod, A. Faust, A. Zaban and U. Banin, *ACS Nano,* 2010, **4**, 5962−5968.
29 Z. Pan, H. Zhang, K. Cheng, Y. Hou, J. Hua and X. Zhong, *ACS Nano,* 2012, **6**, 3982.
30 I. Mora-Seró, S. Giménez, T. Moehl, F. Fabregat-Santiago, T. Lana-Villareal, R. Gomez and J. Bisquert, *Nanotechnology,* 2008, **19**, 424007.
31 H. Zhao, Z. Fan, H. Liang, G. S. Selopal, B. A. Gonfa, L. Jin, A. Soudi, D. Cui, F. Enrichi, M. M. Natile, I. Concina, D. Ma, A. O. Govorov, F. Rosei, and A. Vomiero, *Nanoscale*, 2014, **6**, 7004.
32 D. Wang, H. G. Zhao, N. Wu, M. A. Elkhakani, and D. Ma, *J. Phys. Chem. Lett.,* 2010, **1**, 1030–1035.
33 N. Guijarro, T. Lana-Villarreal, I. Mora-Seró, J. Bisquert and R. Gómez, *J. Phys. Chem. C,* 2009, **113**, 4208–4214.
34 P. Sarkar and P.S. Nicholson, *J. Am. Ceram. Soc.,* 1996, **79**, 1987–2002.
35 A. R. Boccaccini, J.A. Roether, B.J.C. Thomas, M. S. P. Shaffer, E. Chavez, E. Stoll and E. J. Minay, *J. Ceram. Soc. Jpn*., 2006, **114** (1), 1–14.
36 H. W. Chen, Y. T. Liao, J. G. Chen, K. C. W. Wu and K. C. Ho, *J. Mater. Chem.,* 2011, **21**, 17511-17518.
37 M. Tsutomu and K. Yujiro, *J. Electrochem. Soc.,* 2004, **151** (11), 1767-1773.
38 S. Uchida, M. Timiha, H. Takizawa and M. Kawaraya, *J Photochem Photobiol A:* Chem, 2004, **164**, 93–96.
39 H. W. Chen, C. P. Liang, H. S. Huang, J. G. Chen, R. Vittal, C. Y. Lin, K. C. W. Wu and K. C. Ho, *Chem. Commun.,* 2011,**47**, 8346–8348.
40 M. E. Wong and P. C. Searson, *Appl. Phys.Lett.,* 1999, **74**, 2939–2941.
41 S. V. Mahajan, J. Cho, M. S. P. Shaffer, A. R. Boccaccini and J. H. Dickerson, *J. Eur. Ceram. Soc.* 2010, **30**, 1145–1150.
42 M. Giersig, P. Mulvaney, *J. Phys. Chem.,* 1993, **97**, 6334–6336.
43 M. N. Patel, R. D. Williams, R. A. May, H. Uchida, K. J. Stevenson, K. P. Johnston, *Chem. Mater.,* 2008, **20**, 6029–6040.

44 L. Grinis, S. Dor, A. Ofir, A. Zaban, *J. Photochem. Photobiol. A,* 2008, **198**, 52–59.

45 B. Ferrari, A. Bartret, C. Baudin, *J. Eur. Ceram. Soc.,* 2009, **29**, 1083–1092.

46 M. Vidotti and S. I. C. de Torresi, *Electrochim. Acta,* 2009, **54**, 2800–2804.

47 N. J. Smith, K. J. Emmett and S. J. Rosenthal, *Appl. Phys. Lett., 2008,* **93**, 043504.

48 N. P. Benehkohal, V. González-Pedro, P. P. Boix, S. Chavhan, R. Tena-Zaera, G. P. Demopoulos, and I. Mora-Seró, *J. Phys. Chem. C*, 2012, **116** (31), 16391–16397.

49 I. Hod, V. González-Pedro, Z. Tachan, F. Fabregat-Santiago, I. Mora-Seró, J. Bisquert and A. Zaban, *J . Phys. Chem. Lett.*, 2011, ***2*** (24), 3032–3035.

50 K. Szendrei, M. Speirs, W. Gomulya, D. Jarzab, M. Manca, O. V. Mikhnenko, M. Yarema, B. J. Kooi, W. Heiss and M. A. Loi, *Adv. Funct. Mater.*, 2012, **22**, 1598–1605.

51 J. Tang, K. W. Kemp, S. Hoogland, K. S. Jeong, H. Liu, L. Levina, M. Furukawa, X. H. Wang, R. Debnath, D. K. Cha, K. W. Chou, A. Fischer, A. Amassian, J. B. Asbury, E. H. Sargent, *Nat. Mater.,* 2011, **10** (10), 765–771.

52 B. O. Dabbousi, J. Rodriguez-Viejo, F. V. Mikulec,; J. R. Heine, H. Mattoussi, R. Ober, K. F. Jensen, M. G. Bawendi, *J. Phys. Chem. B,* 1997, **101** (46), 9463–9475.

53 L. Dworak, V. V. Matylitsky, V. V. Breus, M. Braun, T. Basche, J. Wachtveitl, *J. Phys. Chem. C,*, 2011, **115** (10), 3949–3955.

54 H. Zhao, T. Zhang, M. Chaker, and D. Ma. *J. Nanoscience Nanotechnology,* 2010, **10**, 4897–4905.

55 A. H. Ip, S. M. Thon, S. Hoogland, O. Voznyy, D. Zhitomirsky, R. Debnath, L. Levina, L. R. Rollny, G. H. Carey, A. Fischer, K. W. Kemp, I. J. Kramer, Z. Ning, A. J. Labelle, K. W. Chou, A. Amassian and E. H. Sargent, *Nat. Nanotechnol.*, 2012, **7**, 577–582.

56 M. Pietryga, D. J. Werder, D. J. Williams, J. L. Casson, R. D. Schaller, V. I. Klimov, and J. A. Hollingsworth, *J. Am. Chem. Soc.,* 2008, **130**, 4879–4885.

57 H. Zhao, M. Chaker, and D. Ma. *J. Mater. Chem.* 2011, **21**, 17483–17491.

58 H. G. Zhao, M. Chaker, N. Q. Wu and D. Ma, *J. Mater. Chem.* 2011, **21** (24), 8898–8904.

59 T. Zhang, H. G. Zhao, D. Riabinina, M. Chaker, D. Ma, *J. Phys. Chem. C,* 2010, **114** (22), 10153–10159.

60 H. G. Zhao, D. F. Wang, T. Zhang, M. Chaker, D. Ma, *Chem. Comm.* 2010, **46** (29), 5301–5303.

61 M. A. Islam, Y. Q. Xia, D. A. Telesca, M. L. Steigerwald, I. P. Herman, *Chem.Mater.* 2004, **16**, 49–54.

62 R. Krishnan, M. A. Hahn, Z. Yu, J. Silcox, P. M. Fauchet and T. D. Krauss, *Phys. ReV. Lett.* 2004, **92** (21), 216803(1)-216803(4).

63 G. Kalyuzhny and R. W. Murray, *J. Phys. Chem. B*, 2005, **109**, 7012-7021.

64 H. Mehrer, Analysis and Simulation of Semiconductor Devices, 2007, **ISSN 0171-1873**, ISBN 978-3-540-71486-6.